



Research
Energy System Engineering—Article

Crack-Net: A Deep Learning Approach to Predict Crack Propagation and Stress–Strain Curves in Particulate Composites



Hao Xu ^{a,b,#}, Wei Fan ^{c,#,*}, Lecheng Ruan ^d, Rundong Shi ^e, Ambrose C. Taylor ^c, Dongxiao Zhang ^{f,g,*}

^a Zhejiang Key Laboratory of Industrial Intelligence and Digital Twin, Eastern Institute of Technology, Ningbo 315200, China

^b BIC-ESAT, ERE, and SKLTCS, College of Engineering, Peking University, Beijing 100871, China

^c Department of Mechanical Engineering, Imperial College London, South Kensington Campus, London SW7 2AZ, UK

^d Department of Mechanical and Aerospace Engineering, University of California, Los Angeles, CA 90095, USA

^e Meituan Corporate, Beijing 100020, China

^f Ningbo Institute of Digital Twin, Eastern Institute of Technology, Ningbo 315200, China

^g Department of Mathematics and Theories, Peng Cheng Laboratory, Shenzhen 518000, China

ARTICLE INFO

Article history:

Received 26 August 2024

Revised 13 December 2024

Accepted 11 February 2025

Available online 8 April 2025

Keywords:

Fracture of composites

Crack evolution

Deep learning

Modeling

ABSTRACT

Computational solid mechanics has become an indispensable approach in engineering, and numerical investigation of fracturing in composites is essential, as composites are widely used in structural applications. Crack evolution in composites is the path to elucidating the relationship between microstructures and fracture performance, but crack-based finite-element methods are computationally expensive and time-consuming, which limits their application in computation-intensive scenarios. Consequently, this study proposes a deep learning framework called Crack-Net for instant prediction of the dynamic crack growth process, as well as its strain–stress curve. Specifically, Crack-Net introduces an implicit constraint technique, which incorporates the relationship between crack evolution and stress response into the network architecture. This technique substantially reduces data requirements while improving predictive accuracy. The transfer learning technique enables Crack-Net to handle composite materials with reinforcements of different strengths. Trained on high-accuracy fracture development datasets from phase field simulations, the proposed framework is capable of tackling intricate scenarios, involving materials with diverse interfaces, varying initial conditions, and the intricate elastoplastic fracture process. The proposed Crack-Net holds great promise for practical applications in engineering and materials science, in which accurate and efficient fracture prediction is crucial for optimizing material performance and microstructural design.

© 2025 THE AUTHORS. Published by Elsevier LTD on behalf of Chinese Academy of Engineering and Higher Education Press Limited Company. This is an open access article under the CC BY-NC-ND license (<http://creativecommons.org/licenses/by-nc-nd/4.0/>).

1. Introduction

Fracturing is one of the most common failure modes in engineering applications, making the numerical prediction of ruptures based on microstructural information highly significant. This problem is especially urgent and complex in composites, which are extensively used in aerospace, automotive, watercraft, wind turbine, and other applications. The modeling of crack evolution using composite representative volume elements (RVEs) plays a key role

in bridging our knowledge of microstructure and that of fracture properties, understanding the fracture mechanisms, and facilitating material design. Compared with fracturing in homogeneous solids, crack evolution in composites is markedly more complicated because of the discontinuous material properties and subsequent various toughening mechanisms, such as crack branching, crack bridging, and crack pinning [1,2]. Crack-based finite-element methods (FEMs), such as the cohesive zone model [3,4], singular element model [5,6], local/nonlocal damage model [7–10], extended FEM [11–13], crack phase field approach [14–17], fracture-based multiscale models [18–22], and peridynamics [23,24], have been widely investigated, and remarkable insights into the fracture process have been obtained through these simulations. However, the performance of finite-element (FE) models

* Corresponding authors.

E-mail addresses: w.fan19@imperial.ac.uk (W. Fan), dzhang@eitech.edu.cn (D. Zhang).

These authors contributed equally to this work.

is highly dependent on fine element sizes and small increment sizes, which are always computationally demanding and time-consuming. The shortcoming of expensive computation are augmented further when batches of simulations are necessary, such as high-throughput computation for the screening and optimization of composite compositions.

In recent years, artificial intelligence (AI) models trained on simulation data have attracted increasing attention due to their remarkable capacity for predicting the mechanics of materials. Deep neural networks (DNNs) have been commonly used in computational mechanics to provide direct predictions from the undeformed microstructural RVE to the desired outputs, such as mechanical properties [25–28], stress–strain curves [29–36], stress fields [37–40], and crack patterns [41–43], and good agreement has been demonstrated between these predictive models and the results from FE simulations. Despite achieving robust and accurate predictions in various tasks, these DNN models were inherently designed for end-to-end predictions, such as image classification, which presents two concerns in physical prediction: the huge demand for data and the exclusion of processing information. DNN models are naturally data-requesting, but current training practices only utilize initial and final information from a simulation, leading to a high simulation cost. For example, predictions of stress–strain curves in composites are meaningful, as the fracture properties of a material are always decided by the weakest defect in the sample. Consequently, the inelastic properties of the cracked material, such as strength and toughness, can only be obtained from the full stress–strain curve. However, the development of a predictive model generally necessitates a substantial dataset, often ranging from several thousand to tens of thousands of individual cases [29–33]. In addition, the lack of processing information indicates that the crack evolution is undetectable, while it is crucial in fracture mechanics, as discussed above.

Alternatively, spatiotemporal dynamical frameworks represented by physics-informed neural networks (PINNs) have become a new type of surrogating FE model [44–48]. In this approach, spatial crack propagation in homogeneous and brittle solids is captured by the PINN solver for partial differential equations (PDEs) under varied initial/boundary conditions [49–51], and time marching is achieved by looping the PDE solver. Inclusion of the physical model significantly reduces the training data size and provides physical support for the predictions. However, discontinuous material properties and non-convex problems, such as energy evolution [52,53], can be great challenges for a PINN, and these two features are fundamental in fractures of composites. Moreover, PINN performance relies heavily on a delicately crafted model that incorporates explicit numerical equations. As mentioned above, fracture problems comprising different conditions require different numerical frameworks, such that substantial efforts are required to build a PINN. As mentioned above, understanding crack evolution in composites constitutes the key step to bridge the gap between microstructure and fracture performance. Although DNN-based crack path predictions in fiber-reinforced composites (FRCs) have been studied [37,41,42], these models are unsuitable for complicated crack patterns, such as when a rupture of the secondary phase is involved. Furthermore, crack evolution predictions in these studies do not contribute to the prediction of mechanical properties, such as stress–strain curves.

Therefore, the core problem is as follows: How can the whole fracture evolution process in a complicated composite material be predicted with limited training data? As illustrated in Fig. 1(a), the crack phase field d_k and corresponding stress σ_k in all time steps should be predicted from a given microstructure. This work proposes a deep learning approach called Crack-Net that manages to simultaneously predict discontinuous crack propagation and non-convex stress–strain behavior in composites. Unlike

PINNs, which employ explicit physical constraints, Crack-Net adopts an implicit constraint technique in which the relationship between crack evolution and stress response is incorporated into the network architecture, as illustrated in Fig. 1. For the prediction of the dynamic fracture process, a spatiotemporal dynamical strategy is employed, in which the model merely predicts short-term crack patterns (spatial information), while the prediction of long-term crack evolution and stress–strain behavior (time marching) are achieved by looping the model. This strategy effectively reduces the demand for training datasets by up to two orders of magnitude, necessitating only hundreds of simulations. Moreover, the proposed framework just needs to be trained once to predict the crack evolution and stress–strain curve simultaneously (Fig. 1 (a)). In this way, Crack-Net is capable of tackling various intricate situations, such as different geometries and material compositions.

The remainder of this paper is organized as follows: In Section 2, the methodology of the proposed framework is introduced in detail, along with the preparation of datasets through numerical simulation. In Section 3, the performance of the proposed Crack-Net in predicting the crack evolution and stress–strain curve is examined under different conditions, including diverse interfaces, varying initial conditions, as well as the intricate elastoplastic fracture process. In Section 4, which concludes this paper, the advantages and limitations of the proposed Crack-Net are summarized.

2. Materials and methods

2.1. Morphology development from phase separation simulation

An A–B binary composite system resulting from the phase separation of miscible polymer blends presents good interfacial adhesion between the components, which enhances the overall mechanical performance. The generating morphologies are usually divided into two types—that is, particle-reinforced composites (PRCs) and interpenetrating phase composites (IPCs)—depending on the initial compositions, c_{A0} and c_{B0} , where $c_{A0} + c_{B0} = 1$. The morphology evolution is governed by the Cahn–Hilliard equation [54]:

$$\frac{\partial c_B}{\partial t} = M \Delta \left[\frac{df(c_B)}{dc_B} - \gamma \Delta c_B \right] \quad (1)$$

where c_B is the concentration of component B, t is time, M is the mobility coefficient, γ is a constant regarding interphase thickness, and $f(c_B)$ is a free energy density function.

In the current study, a $100 \mu\text{m} \times 100 \mu\text{m}$ domain was meshed into identical square elements with element size h_{FEM} , where $h_{\text{FEM}} = 1 \mu\text{m}$, for the numerical simulation (Fig. 2(a)). An open-source FEniCS algorithm [55,56] was employed to generate the morphology, and periodic boundary conditions were applied to the domain (Fig. 2(b)). The following parameters were set: time step $dt = 5 \times 10^{-6}$ s, mobility $M = 1 \text{ m}^2 \cdot \text{s}^{-1}$, $\gamma = 0.01 \text{ m}^2 \cdot \text{s}^{-1}$, and $f(c_B) = 100 \cdot c_B^2 \cdot (1 - c_B)^2$. An initial c_B value was randomly assigned with a normal distribution $N(c_{B0}, 0.01)$ to each element at $t = 0$. By varying c_{B0} from 0.25 to 0.50, the morphology varies from PRC to IPC, as shown in Fig. 2(c). The volume fractions of the A-rich phase, $V_{f,A}$, and the B-rich phase, $V_{f,B}$, were controlled by a cut-off value of concentration, and different cut-off values were selected for different c_{B0} series. Detailed information is provided in Table S1 in Appendix A.

2.2. Fracture simulations and dataset generation

The resulting specimens were then subjected to fracture simulations by taking the A-rich phase as the matrix and the B-rich phase as the modifier. An edge pre-cut was introduced to the matrix. Since the morphology was randomly generated, specimens in which the crack tip was located in the B-rich phase were not

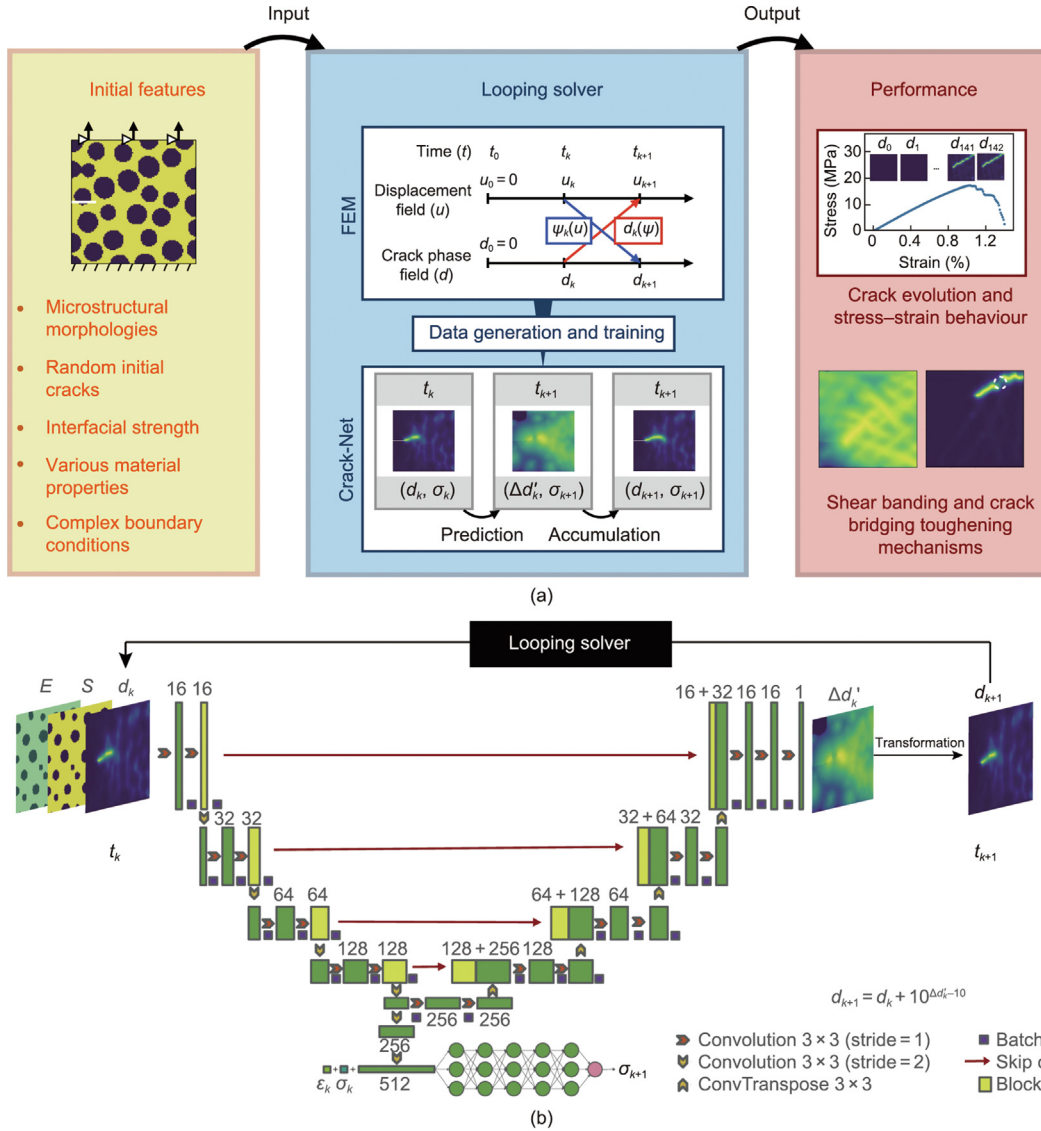


Fig. 1. The Crack-Net framework. (a) An illustrative map for Crack-Net, including the initial features, looping solver for data generation, model training, and prediction performance. (b) The Crack-Net architecture, which utilizes the composite design, fracture phase field, strain, and stress in the current step to predict the transformed increment of the fracture phase field and stress in the next step, which are coupled by the same latent vector. Here, E is modulus and S is strength.

used. The bottom of the specimens was encastre. The top of the specimens was constrained horizontally and stretched vertically with a constant increment size $10^{-3} \mu\text{m}$ (Fig. 2(b)). The left and right boundaries were without constraints.

The phase field method by Gergely Molnár et al. [57] was adopted to simulate the crack evolution process in the domain, where a crack was described by a continuous scalar $d \in [0, 1]$, with $d = 0$ indicating the pristine material, and $d = 1$ indicating the ruptured state. Obviously, the crack phase field d is similar to the damage variable in terms of continuum damage mechanics, which is used to degrade the material stiffness. A detailed description about the constitutive behavior is given in Section S1.1 in the Appendix A.

During the implementation, either an elastic response or an elastoplastic response can be selected using a plastic switch. For elastic elements, the constitutive behavior is controlled by the tensile modulus E , fracture parameter g_c , and characteristic crack width $l_c = 2h_{\text{FEM}}$. The material strength, S , is determined by the maximum stress from a uniaxial tension of a single element with given parameters (E, g_c, l_c). For elastoplastic elements, in addition to the above parameters, the yielding stress Y , hardening modulus

H , and elastic threshold are also applied. To implement this method in Abaqus, three layers of the meshing grid were connected through the same nodes, and different element types were adopted for different purposes. The displacement problem and damage problem were solved using four-node plane strain element (CPE4) elements and user-defined elements, respectively, and visualization was achieved using zero-stiffness elements. The crack phase field value of each element is calculated as the average value from four integration point values.

It is important to note that the fracture parameter g_c is different from the fracture energy, although both control the crack evolution and have the same unit. The relationship between these two parameters is given by the following:

$$\text{Fracture energy} = \int_{\Omega} g_c \left(\frac{1}{2l_c} d^2 + \frac{l_c}{2} |\nabla d|^2 \right) d\Omega \quad (2)$$

where d is the crack phase field, ∇d is the gradient of crack phase field, and l_c is the characteristic crack width.

Both the cases with and without an interface are considered. In Sections 3.1 and 3.2, perfect bonding between the A phase and B

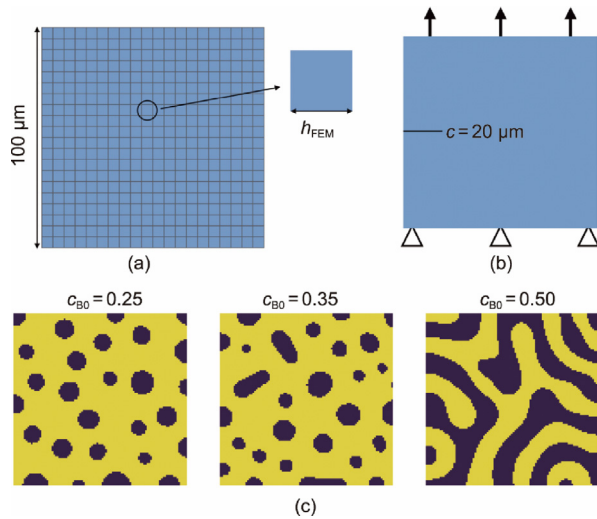


Fig. 2. Schematic of the simulation set-up. (a) The meshing elements in the numerical simulation, $h_{FEM} = 1 \mu\text{m}$ during simulations and $h_{FEM} = 5 \mu\text{m}$ here, for clear viewing. (b) The boundary conditions of simulations. (c) Examples of the generated morphology with c_{B0} ranging from 0.25 to 0.50.

phase is assumed. In Sections 3.3 and 3.4, the single-layer element between the matrix and fillers is assigned as an interface with elastic constitutive behavior. The strong interface (modulus $E_{IF} = 5000 \text{ MPa}$, fracture parameter $g_{clF} = 10 \text{ J}\cdot\text{m}^{-2}$, strength $S_{IF} = 35.0 \text{ MPa}$) and weak interface (modulus $E_{IF} = 5000 \text{ MPa}$, fracture parameter $g_{clF} = 1 \text{ J}\cdot\text{m}^{-2}$, strength $S_{IF} = 10.8 \text{ MPa}$) are both examined. The modulus of the modifiers was changed accordingly, as displayed in Tables S1 and S2 in Appendix A. For each simulation, the processing data—including the overall applied stress and crack phase field map—were extracted at an output frequency of 10 or incremental strain of 0.01%. Finally, the initial morphology information of the composite microstructure, the component model parameters, and the processing information, such as the overall stress–strain curve and crack phase field, consist of the training dataset. Additional information regarding phase field methods can be found in previous works [2,14–17].

The implementation of the crack phase field method is accomplished by means of Abaqus. A soft but tough core was generalized to mimic the behavior of as wide a range of particles as possible. A yielding stress Y with no hardening modulus was adopted to limit the strength of the core. The core–shell interface and shell–matrix interface were assumed to be perfectly bonded. The modulus and fracture parameter of the matrix were fixed at 4 GPa and $1 \text{ J}\cdot\text{m}^{-2}$, respectively, to fit the stress–strain behavior of pure epoxy. The material parameters, including the shell modulus E_{shell} , shell toughness $g_{c,shell}$, core modulus E_{core} , core yielding stress Y_{core} , and core–shell size ratio r_c/t_s , were varied, and their effects are explored in Section 3. The effects and validation of the material parameters are discussed in Section S1.2 in Appendix A, and the model parameters of individual components and the stress–strain curves of different materials are displayed in Figs. S1 and S2 in Appendix A. A rupture criterion stress $\sigma_{rup} = 0.5 \text{ MPa}$ was applied, since considering computation after this critical point is redundant.

2.3. The architecture design of Crack-Net

The proposed Crack-Net adopts a specialized architecture modeled on U-Net, featuring an encoder-decoder design. U-Net, originally developed for medical image segmentation, has gained widespread popularity due to its remarkable performance and versatility in various applications [58,59]. In the U-Net architecture,

the encoder part utilizes a series of convolutional layers to extract hierarchical features from the input data, gradually reducing its spatial dimensions while capturing intricate patterns. The decoder part then employs up-convolutional layers to expand the extracted features and reconstruct the output with the same spatial dimensions as the input. One of the key advantages of U-Net lies in its ability to preserve spatial information during the encoding and decoding process. This characteristic ensures that the fine details and localized features of the input data are retained in the output, making it particularly effective for certain tasks such as image segmentation and object detection. The skip connections between corresponding encoder and decoder layers further enhance the model's capability to capture both low-level and high-level features, thus facilitating precise predictions.

In this work, numerical simulations with 100×100 elements are investigated. It is worth noting that any other resolution ratios of elements can also be input into Crack-Net through a resizing layer. As illustrated in Fig. S4 in Appendix A, given other resolution ratios of elements, Crack-Net can also provide accurate predictions. A comparison of the mechanical properties of different resolution ratios is displayed in Table S3 in Appendix A; the results demonstrate that the modulus and tensile strength are not significantly affected by the model size. In Crack-Net, the size of the input is $3 \times 100 \times 100$, including the initial elastic modulus matrix (\mathbf{E}_0), ultimate tensile strength matrix (\mathbf{S}), and current crack phase field matrix (\mathbf{d}_k), which are all fields with the size of 100×100 . The size of the output is the transformed increment of the crack phase field $\Delta d_k'$ with a size of $1 \times 100 \times 100$. The network architecture is presented in Fig. 1(b), and detailed descriptions are provided in Section S1.2. The architecture described above is similar to the conventional U-Net structure, which aids in reconstructing the transformation increment of the predicted crack phase field.

However, our Crack-Net goes beyond this initial reconstruction and implements further processing on the latent vector extracted by the encoder. This crucial step enables the model to achieve simultaneous prediction of the stress and crack phase field, making it specialized for precise crack propagation prediction in composite materials. As shown in Fig. 1(b), the extracted latent vector is sent into an additional feature extraction block to further extract the information. Consequently, the output of the feature extraction block is a 512-dimensional vector containing high-dimensional latent information concerning the input composite morphology and the current crack phase field. To further predict the stress in the subsequent step, this 512-dimensional vector is combined with the strain and stress from the current step and fed into a fully connected artificial neural network (ANN). This sophisticated process enables Crack-Net to accurately predict the stress response in the next step. To embed the initial conditions into Crack-Net, the inputs of the neural network were refined. To be specific, the values of strength (S) and initial modulus (E_0) at the precut location were designated as zero, which allowed us to explicitly encode both the positional and length-based information of the precut within the network's input structure. It is important to emphasize that the predicted stress and crack phase field for the subsequent step originate from the same latent vector extracted from the encoder part of Crack-Net. This design enables the network to capture the underlying relationship between crack propagation and strain development, increasing the accuracy and physical coherence of the predictions.

2.4. Long-term prediction procedure by Crack-Net

Although Crack-Net is trained by short-term data, the relationship between the input and output makes it able to make long-term predictions by incrementally predicting the next step from the previous prediction. In this section, the procedure of

Crack-Net's long-term prediction is detailed. As shown in Algorithm 1, long-term prediction only requires the initial situation and the composite morphology. Without any prior information, Crack-Net is directly employed to predict the crack propagation starting from the initial step, where the fracture has not yet initiated. From Algorithm 1, it is evident that Crack-Net possesses the ability to predict the transformed increment, which is subsequently converted back to the absolute increment and added to the phase field in the current step to obtain the phase field for the subsequent step. Additionally, the stress in the next step is directly predicted by Crack-Net. Given the fixed interval of the strain ratio, the strain ratio in each step can be calculated, making it possible to acquire the state for the subsequent step from Crack-Net's predictions. This process forms a loop that can be iterated until the maximum value set beforehand is reached. As observed from the long-term prediction process, Crack-Net can predict the crack phase field and stress at each step of the fracture process, based on the given composite morphology. Remarkably, Crack-Net possesses the flexibility to predict from any step of the fracture by simply altering the initial state in Algorithm 1 to match the desired step's state.

The initial crack phase field is termed as $(d_0, \sigma_0, \varepsilon_0)$, where d_0 is the initial crack phase field matrix filled with 0, while σ_0 and ε_0 are 0. The initial state is fed into Crack-Net to predict the subsequent step's state, which is then used as input to predict the preceding steps' states of cracking. The formula can be written as follows:

$$\left(\hat{d}_k, \hat{\sigma}_k, \hat{\varepsilon}_k\right) \xrightarrow{\text{Crack-Net}} \left(\hat{d}_{k+1}, \hat{\sigma}_{k+1}, \varepsilon_k + \Delta\varepsilon\right) \quad (3)$$

$$\hat{d}_{k+1} = \hat{d}_k + 10^{\Delta\hat{d}'_k - 10} \quad (4)$$

The detailed procedure of the long-term process is provided Algorithm 1. Apart from predetermined composite information, Crack-Net can generate predictions without requiring additional conditions or historic states, which increases its practical applicability.

2.5. Implements for training Crack-Net

A spatiotemporal dynamical workflow is designed to predict the mechanical performance and crack growth path of composites under tensile displacement control. In the framework, the continuous fracture process of PRC RVEs is evenly divided into discrete frames, and each frame is characterized by the spatial crack pattern and the stress applied to the whole domain. Accordingly, a hierarchical approach is proposed—that is, short-term spatial predictions and long-term time marching. In the short-term hierarchy, the spatial crack pattern and overall stress at step k are predicted based on the information from step $(k-1)$ via the end-to-end Crack-Net model rather than solving PDEs; at the long-term loop, the Crack-Net model is called incrementally to generate the whole fracture process of composite RVEs from the undeformed state to the rupture state. The architecture of the end-to-end Crack-Net (short-term predictions) is displayed in Fig. 1(b).

The training dataset comprising 554 cases was obtained through phase field simulations [2] on a 100×100 -element PRC domain, and the cracks are described by a continuous scalar crack phase field $d \in [0, 1]$, where $d = 0$ indicates the intact material, and $d = 1$ indicates a fully broken state (Section 2.2). Herein, our focus has primarily been on configurations comprising 100×100 elements. This resolution offers a good balance between illustrating crack propagation patterns with sufficient clarity and maintaining acceptable computational demands. It is worth mentioning that models with higher resolutions that incorporate more precise details can also be trained using a similar methodology.

Algorithm 1: Long-term prediction via Crack-Net

Initial:	$(d_0, \sigma_0, \varepsilon_0), \Delta\varepsilon = 1\%, S$ and E_0 are constant fields
1st step:	$(d_0, \sigma_0, \varepsilon_0) \xrightarrow{\text{Crack-Net}} (\Delta\hat{d}'_0, \hat{\sigma}_1)$ $\hat{d}_1 = d_0 + 10^{\Delta\hat{d}'_0 - 10}$ $\varepsilon_1 = \varepsilon_0 + \Delta\varepsilon$ Get the prediction $(\hat{d}_1, \hat{\sigma}_1, \varepsilon_1)$
Loop:	$(\hat{d}_k, \hat{\sigma}_k, \varepsilon_k) \xrightarrow{\text{Crack-Net}} (\hat{d}_{k+1}, \hat{\sigma}_{k+1})$ $\hat{d}_{k+1} = d_k + 10^{\Delta\hat{d}'_k - 10}$ $\varepsilon_{k+1} = \varepsilon_k + \Delta\varepsilon$ Get the prediction $(\hat{d}_{k+1}, \hat{\sigma}_{k+1}, \varepsilon_{k+1})$ Until stress decreases to be lower than a threshold ($< 5\%$ of maximum stress) and maintains for several steps

The incremental strain $\Delta\varepsilon$ of 0.01% was applied to partition the fracture process, and 83 480 step pairs were extracted from the 554 simulation cases. Here, the step pairs refer to the input stress and crack phase field in the current step, and to the referred output stress and crack phase field in the subsequent step. The step pairs were then divided into three sets, allocating 80% for training (66 784 steps), 10% for validation (8348 steps), and another 10% for testing (8348 steps) purposes. The training process involved 3000 epochs with a batch size of 100; to prevent overfitting, an early stopping technique was used. Importantly, the dataset was randomly split based on the step in the slice prediction. In the dataset, the spatial distribution of matrix phase A and reinforcing phase B is characterized by the material parameters in the matrix (matrix modulus $E_A = 5000$ MPa, matrix strength $S_A = 35$ MPa, filler modulus $E_B = 500$ MPa, filler strength $S_B = 10.8$ MPa). The resulting morphology patterns in the training process are illustrated in Fig. S5 in Appendix A, which shows that the minutiae of the prediction become more apparent as the training epoch increases.

Apparently, precise incremental predictions from step to step are essential to the long-term process of Crack-Net. The strain increment between steps, $\Delta\varepsilon$, is 0.01%. An investigation of the influence of the strain increment on the model's performance is provided in Fig. S6 in Appendix A, showing that a higher strain increment leads to a corresponding increase in predictive error. The differences in the crack phase field between steps are generally subtle, particularly during the initial and final stages of fracture development, where the difference of the crack phase field usually ranges from 10^{-2} to 10^{-5} . Here, instead of the crack phase field matrix, d , a transformed incremental value matrix, $\Delta d'$, is predicted. For each element, as the value of d is between 0 and 1 and continues to monotonically increase from step k to step $(k+1)$, $\Delta d_k = d_{k+1} - d_k$ is usually a tiny number between 0 and 1. Therefore, log transformation is adopted to amplify minor differences in the crack phase field, and the transformed incremental crack phase field, $\Delta d'_k$ is defined as follows:

$$\Delta d'_k = 10 + \log_{10} \left(\max \left(10^{-10}, d_{k+1} - d_k \right) \right), 0 \leq \Delta d'_k \leq 10 \quad (5)$$

This approach manages to capture the fine-grained details of crack propagation, enabling Crack-Net to make more precise and reliable predictions in scenarios in which the development of the crack phase field is subtle. Consequently, the input of Crack-Net involves the initial elasticity modulus matrix (E), ultimate tensile strength matrix (S), crack phase field matrix (d_k), and the applied

strain (ε_k) and stress (σ_k) in step k . The output is the applied stress in the next step (σ_{k+1}) and the transformed increment of the crack phase field $\Delta d'_k$.

2.6. Transfer learning for Crack-Net

Transfer learning is a machine learning technique in which knowledge gained from solving one task (the source domain) is utilized to improve the performance of another related task (the target domain) [60]. In transfer learning, a pretrained model that has been trained on a large dataset in the source domain is adapted and fine-tuned for a target domain with a smaller dataset. The basic idea behind transfer learning is that the knowledge learned by a model in the source domain can be generalized and applied to the target domain, even if the target domain has a different dataset or distribution. By leveraging the knowledge from the source task, the model can start with a good initial configuration and then fine-tune its parameters on the target task to achieve better performance with less data and training time. In the context of Crack-Net, transfer learning plays a pivotal role in enhancing the model's predictive capabilities for composite materials with varying material properties. Parameter transfer learning is adopted in this work, which utilizes the learned parameters of a pretrained model from the source domain to initialize or fine-tune the model for the target domain. When applying transfer learning, the parameters of the pretrained model are transferred to the target domain; then, the model is further trained using the target domain's data to adapt it to the specific characteristics of the new task. In this work, the entire pretrained model, including both the encoder and decoder, is fine-tuned using the data in the target domain. The parameters are updated based on the loss function in the target domain, allowing the model to adjust its representations and learn task-specific patterns. For the fine-tuning process, the training epoch is 1000, the learning rate is reduced to 10^{-4} , the batch size is 100, and the early-stopping technique is used to prevent overfitting. The settings of the numerical experiments conducted in the Results section are detailed in Section S1.3 in Appendix A.

During the transfer learning training, a challenge arose from the significant differences in the S and E_0 of different materials in the composites. Directly inputting these diverse material properties into the network during training could cause the batch normalization layer in Crack-Net to experience substantial changes in the mean and variance of the batch, which could adversely affect the effectiveness of transfer learning. To address this issue, a crucial pre-processing step was implemented for the material properties of the composite materials. Given the correlation between the mode of crack propagation and the relative strength of the matrix and reinforcement phase of the composite material, we applied normalization techniques to bring the material properties in the target domain closer to the order of magnitude in the source domain. By normalizing the material properties, we ensured that their values were scaled appropriately, enabling the transfer learning process to proceed more smoothly. The normalized material properties can be written as follows:

$$S_{\text{target}} = S_{\text{target}} \times \frac{\max(S_{\text{source}})}{\max(S_{\text{target}})} \quad (6)$$

$$E_{\text{target}} = E_{\text{target}} \times \frac{\max(E_{\text{source}})}{\max(E_{\text{target}})} \quad (7)$$

3. Results

In this section, four scenarios are presented to demonstrate the generalization ability of Crack-Net under different conditions. The

effects of crack initiation, interface strength, matrix plasticity, and filler properties are examined, and Crack-Net presents remarkable accuracy and robustness in all scenarios. The experiments were conducted using a computer equipped with an Intel Xeon Gold 5115 CPU and an NVIDIA GeForce RTX 2080 Ti GPU. In this work, the reference results come from the numerical simulations by means of phase field methods.

3.1. Short-term prediction in centrally notched elastic composites with perfect interface

A simplified case of brittle fracture was employed in this section. The matrix phase A was stiff (modulus $E_A = 5$ GPa and tensile strength $S_A = 35$ MPa), and the filler phase B was soft (modulus $E_B = 0.5$ GPa and tensile strength $S_B = 10.8$ MPa). The two phases were assumed to be elastic and perfectly bonded, while the pre-crack was fixed to be $20 \mu\text{m}$ at the center of the edge. The performance of Crack-Net in single-step short-term prediction is examined in this section, since the high accuracy of Crack-Net's short-term prediction is the key to its overall predictive ability. Given Crack-Net's capability to simultaneously predict stress response and crack evolution, the performance of both predictions is examined. As shown in Fig. 3(a), the predicted stress demonstrates an excellent match with the observations from the testing dataset, achieving a remarkable R^2 value of 0.9993 and a small mean squared error (MSE) of 0.0378. The prediction of crack evolution is assessed by the overall relative error of the crack phase field, which is defined as follows:

$$e_d = \left(\frac{\sum_i \sum_j (\hat{d}_{ij} - d_{ij})^2}{\sum_i \sum_j (d_{ij})^2} \right)^{1/2} \quad (8)$$

$$e_{\Delta d'} = \sqrt{\frac{\sum_i \sum_j (\Delta \hat{d}'_{ij} - \Delta d'_{ij})^2}{\sum_i \sum_j (\Delta d'_{ij})^2}} \quad (9)$$

where e_d is the relative error of the predicted phase field \hat{d}_{ij} , $e_{\Delta d'}$ is the relative error of the transformed increment $\Delta \hat{d}'_{ij}$, and i and j are the indices of the row and column in the two-dimensional (2D) field, respectively. When calculating the relative error, the point with a value of 0 is neglected to ensure computational validity. This criterion represents the overall error of discrete points of the computational domain. Considering that points characterized by a small or negligible phase field exist, this measurement is stringent. From Figs. 3(b) and (c), more than 80% of the predictions present $e_d < 1\%$, and almost all predictions present $e_d < 6\%$. Although there is a slight increase in $e_{\Delta d'}$ compared with e_d , the majority remain below 1%, with only a few exceptions exceeding 10%. This effectively demonstrates the efficacy of the strategy of predicting a transformed increment instead of the ultimate phase field. In Crack-Net, where loop prediction is employed for long-term crack evolution, the precision of short-term forecasts is of great importance. The subtle changes in the phase field between steps present a challenge for accurate learning. Nonetheless, by transforming and amplifying these changes, the model's predictive performance is improved.

In order to better demonstrate Crack-Net's short-term prediction capability, we generated new composite designs that are not in the training dataset for out-of-sample prediction. The predictions of the crack phase field at $t = k + 1$, \hat{d}_{k+1} , and the incremental crack phase field between $t = k$ and $t = k + 1$, $\Delta \hat{d}'_k$, are compared with the observations from simulations d_{k+1} and $\Delta d'_k$ for an intuitive illustration.

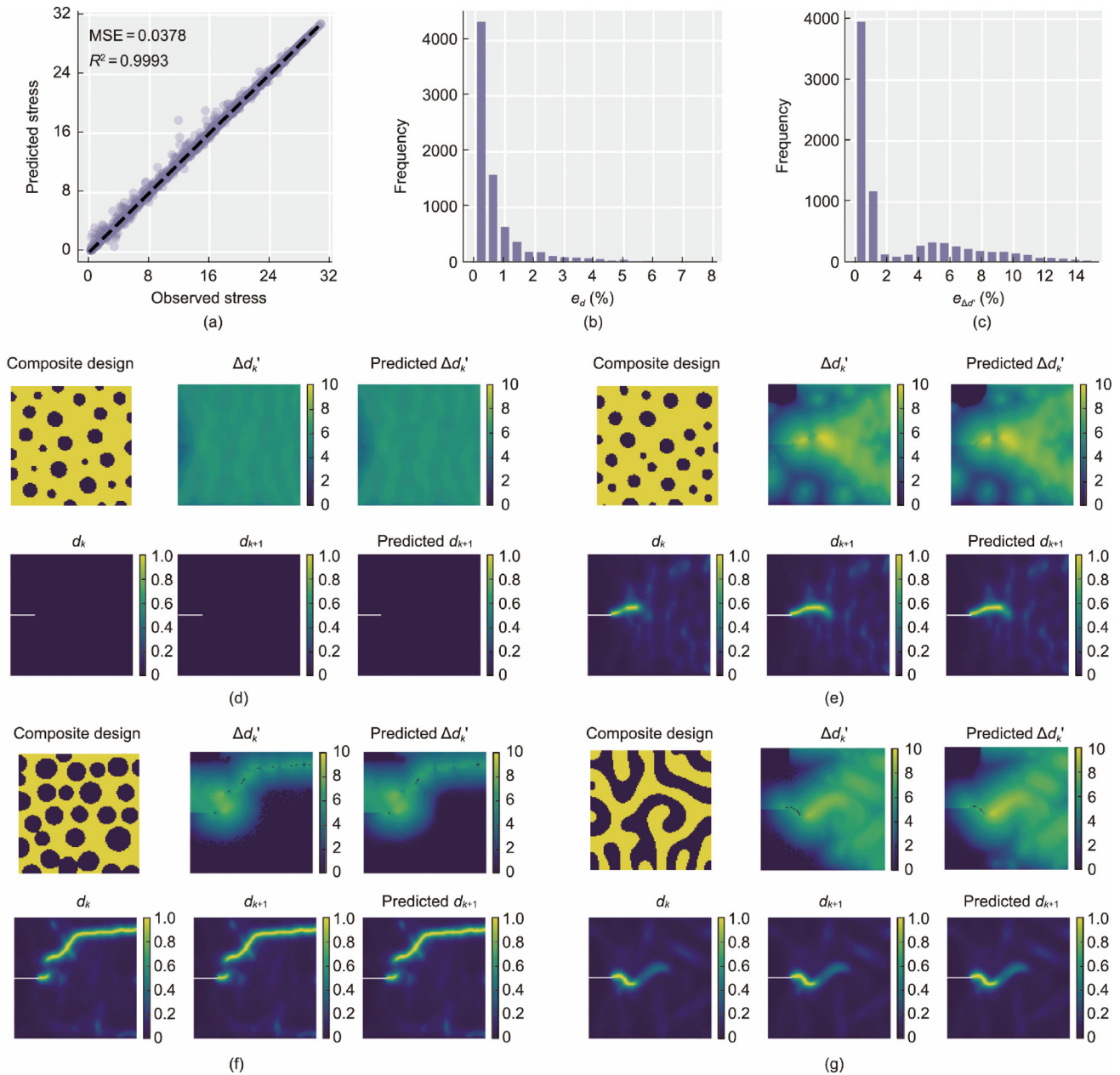


Fig. 3. Single-step short-term prediction by Crack-Net. (a) Predicted and actual (FE) stress in the testing data. (b) Distribution of the relative error of the crack phase field. (c) Distribution of the relative error of the transformed increments of the crack phase field. (d) Out-of-sample prediction in the crack initialization stage where the composite is unbroken. (e) Out-of-sample prediction in the stage of unstable crack growth. (f) Out-of-sample prediction in the last stage of crack propagation. (g) Prediction for binary co-continuous structures. Here, d_k and d_{k+1} are the observed fracture phase field in the current and next step, respectively, and Δd_k^* is the observed transformed increment. The white line in the phase field represents the initial condition.

The predictions for different stages of crack propagation are examined. Fig. 3(d) presents the prediction of crack initiation. At this stage, the material remains unbroken, resulting in a minimal value of the crack phase field. However, the subtle accumulation of increments during this phase plays a critical role in the final crack development. Crack-Net exhibits remarkable accuracy in predicting the distribution of these subtle increments of the crack phase field, which forms a solid foundation for long-term fracture propagation predictions. Fig. 3(e) illustrates the prediction during the unstable crack growth stage. Significant changes in the crack phase field occur between consecutive steps during this stage, which are accurately captured by Crack-Net. The prediction in the last stage of crack propagation is shown in Fig. 3(f), in which the crack has fully grown, and the increment of the crack phase field becomes subtle and clustered near the

crack. It is found that Crack-Net demonstrates precise predictions of this behavior. Notably, the particle size and proportion of the reinforcement phase in Fig. 3(f) are obviously different from those in Figs. 3(d) and (e), highlighting Crack-Net’s generalization ability for diverse composite designs. Moreover, it is observed that, even during the unstable crack growth stage, the changes in the crack phase field between steps are not particularly substantial, which implies that directly predicting the crack phase field may overlook crucial details of these incremental changes. Conversely, the transformed increment exhibits notable variations at each stage of crack propagation, rendering it advantageous for network learning and prediction.

Fig. 3(g) shows excellent agreement between the predictions and observations for the short term in the co-continuous morphology, which features a completely different distribution of the

reinforcement phase. Notably, the Crack-Net training data is exclusively composed of PRC specimens, without encountering co-continuous ones. This indicates that Crack-Net has learned the effect of crack propagation on stress response, which enables it to predict fractures in composites with diverse structural configurations. All these results demonstrate Crack-Net's predictive ability to precisely capture the crack evolution and stress response in the short term.

3.2. Out-of-sample long-term prediction of Crack-Net

With excellent performance on the short-term predictions, Crack-Net was then used to predict the fracture process from the undeformed state to rupture in particulate composites and co-continuous composites. In order to truly reflect the generalization ability of Crack-Net, we conducted out-of-sample prediction, in which several composites with new structure designs are generated for long-term prediction. Notably, these composite designs had never appeared in the training dataset, which meant that they were data outside of the sample; thus, the testing of this data was closer to the practical scenario. The overall stress–strain curves from the reference and predictions are compared in Fig. 4, and the crack patterns from four representative stress–strain points are presented.

In the reference in Fig. 4(a), the stress peaks at point R1 and subsequently declines to point R2 due to crack propagation. From R2 to R3, the crack is hindered by a soft particle (the white circle in crack pattern R3), so the stress increases slightly. It is worth noting that, in many cases, soft particles provide less resistance to crack propagation than the surrounding matrix [61], which is because the stress that the particle undergoes exceeds its strength. In the current case, when the crack just propagates to the interface between the matrix and particle, the soft particle has not reached its rupture strength as it undergoes less stress, and it can hinder the crack until the stress is beyond its strength. This is similar to the crack bridging effect and has been discussed in the literature [2,17,62]. Afterward, the crack propagates unstably, and the final rupture occurs (R4). During this process, the crack evolution is discontinuous and the stress–strain curve is non-convex, which are typical difficulties in the fracture of a composite. Nevertheless, Crack-Net presents impressive accuracy in both crack evolution and stress–strain curves, with a well-established relationship between the two. Fig. 4(b) demonstrates the excellent alignment between the predictions and observations for both the crack propagation process and the stress–strain curve.

In Fig. 4(c), notable changes occur in the particle proportion and size for the reinforcing phase in the composites. Despite slight deviations in the predicted stress–strain curve, the characteristic steps are well captured by Crack-Net—especially the brief stress maintenance between P2 and P3 in Fig. 4(c). The corresponding crack phase field predicted by Crack-Net remains highly accurate, although the crack is predicted to begin slightly earlier than the reference. Moreover, we observed that, in this case, the cracks did not propagate continuously (R2 and P2 in Fig. 4(c)). Instead, independent fracture points were generated at multiple locations, which eventually expanded and connected as the strain ratio increased. Remarkably, Crack-Net accurately captured this intricate fracture mode, demonstrating its ability to effectively predict and understand complex crack dynamics, including non-continuous crack propagation. In order to make the result more convincing, further out-of-sample prediction cases are provided in Figs. S7–S21 in Appendix A. From the figures, it can be observed that Crack-Net's prediction matches well with the reference from the numerical simulation in most of the cases, which confirms that Crack-Net achieves satisfactory performance in the long-term prediction of crack phase fields and stress–strain curves for compos-

ites with different composite morphologies. In practical applications, additional focus is usually given to the fracture characteristics of composite materials instead of specific steps. Therefore, although Crack-Net sometimes predicts the emergence of cracks earlier, this predictive discrepancy remains inconsequential, since Crack-Net captures the characteristics of the crack propagation. Additional discussions are provided in Section S1.4 in Appendix A.

IPCs were then applied to test Crack-Net's generalization ability, as shown in Fig. 4(d). The fracture process presents similar features to the fracture in the particulate morphology. The model achieved excellent predictions on crack evolution but moderate predictions on the stress–strain curve. While it accurately predicted strength, strain at rupture, and fracture toughness (the area under the stress–strain curve), it performed poorly in predicting the evolution of the modulus. Considering that the co-continuous specimens were not included in the training dataset, this performance is quite acceptable, and it can be concluded that Crack-Net has excellent potential to predict fractures among various heterogeneous structures, rather than only particulate composites. We provide more examples in Appendix A to make this claim more convincing: Figs. S22–S24 in Appendix A depict Crack-Net's long-term prediction for two-phase co-continuous composite materials with different composite designs. It is found that Crack-Net exhibits remarkable efficacy in predicting crack propagation, even in the complex scenario of two-phase co-continuous structures. Such structures, which are characterized by distinct reinforcement phases interwoven in a continuous matrix, present intricate crack propagation pathways that can be challenging to predict accurately. However, Crack-Net can handle this challenge, as exemplified by its predictions, which align well with actual crack phase fields and stress–strain curves of these structures.

3.3. Extension to complicated cases

In the preceding investigation, a simplified scenario was employed to examine the effectiveness of the proposed Crack-Net. Within the confines of fixed initial parameters, Crack-Net exhibited a commendable capacity to discern patterns in crack propagation and yield reliable forecasts. The dynamics of real-world applications, however, often introduce variations, such as various fillers, poor interfacial adhesion, and random initial cracks.

The interface between the matrix and fillers plays a vital role in the fracture of composites, often leading to intricate failure mechanisms that demand a nuanced understanding. Given its significance in practical contexts, the performance of Crack-Net under poor interfacial adhesion and random initial cracks was examined. To embed the initial conditions into Crack-Net, the inputs of the neural network were refined. More specifically, the values of S and E at the precut location were designated as zero, which allowed us to explicitly encode both the positional and length-based information of the precut crack within the network's input structure.

In terms of the dataset, 530 distinct cases were generated and split into 80/10/10, where 80% were for training, 10% were for validation, and 10% were for testing. With a learning rate of 5×10^{-4} , Crack-Net was trained by 2000 iterations, and the early-stopping technique was adopted to prevent overfitting. Upon completing the training phase, the refined Crack-Net model was utilized for out-of-sample prediction. Here, newly generated composite morphologies and precut configurations were adopted, neither of which had been encountered during the training process. The results obtained from Crack-Net are presented in Fig. 5. To quantitatively characterize the crack evolution, the cosine similarity of the crack phase field d and the transformed incremental value

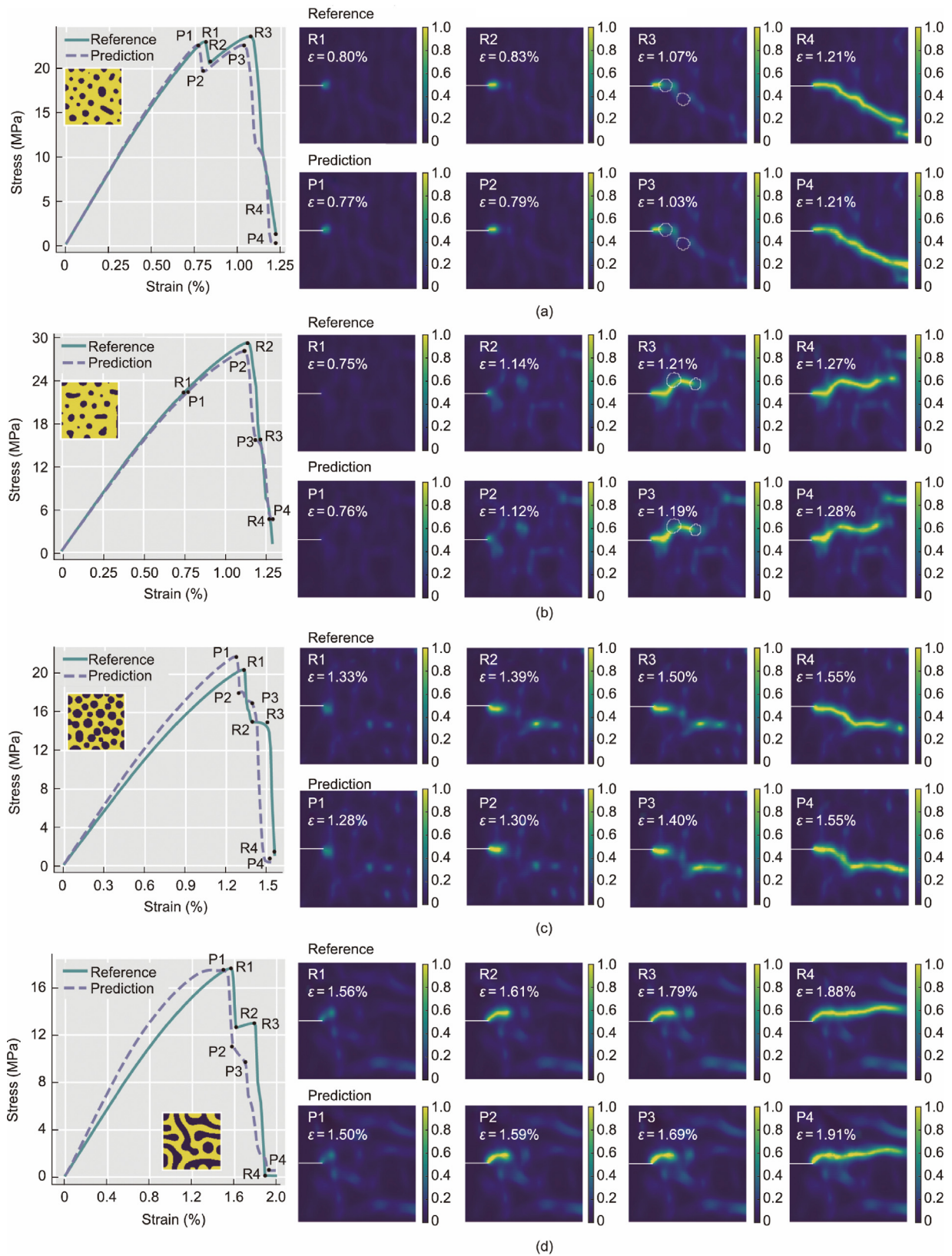


Fig. 4. Long-term prediction by Crack-Net. (a–c) Referred and predicted stress–strain curve (left) and referred (R1–R4) and predicted (P1–P4) phase field at characteristic steps in the stress–strain curves (right) for the particle-reinforcement composite. (d) Referred and predicted stress–strain curve (left) and referred (R1–R4) and predicted (P1–P4) phase field at characteristic steps in the stress–strain curves (right) for the binary co-continuous composite. The composite microstructure design is provided beside the stress–strain curve, where the yellow region is the matrix phase, and the black region is the reinforcement phase. ϵ is the strain ratio. The white line in the phase field represents the initial condition.

$\Delta d'$ under different strains are given in Fig. 5(a); they are calculated as follows:

$$\cos(\theta)_d = \frac{\sum_i \sum_j (d_{ij} \hat{d}_{ij})}{\sqrt{\sum_i \sum_j d_{ij}^2} \sqrt{\sum_i \sum_j \hat{d}_{ij}^2}} \quad (10)$$

$$\cos(\theta)_{\Delta d'} = \frac{\sum_i \sum_j (\Delta d'_{ij} \hat{\Delta d}'_{ij})}{\sqrt{\sum_i \sum_j \Delta d'_{ij}^2} \sqrt{\sum_i \sum_j \hat{\Delta d}'_{ij}^2}} \quad (11)$$

where $\cos(\theta)_d$ and $\cos(\theta)_{\Delta d'}$ are the cosine similarity of the crack phase field d and the transformed incremental value $\Delta d'$, respectively; \hat{d}_{ij} and $\hat{\Delta d}'_{ij}$ are the predictions; and i and j are the indices of row and column in the 2D field, respectively. Here, the range of cosine similarity is between 0 and 1, and a larger cosine similarity corresponds to a higher accuracy of predictions. From the figure, it can be observed that, when the strain is small, the crack has not evolved yet, and the cosine similarity is close to 1. As the strain increases to 0.8%–1.0%, the crack is about to propagate, and the error becomes larger. The median of cosine similarity, however, remains greater than 0.95, indicating accurate overall predictions. The specific work, defined by the area under the stress–strain curve, is also predicted and is presented in Fig. 5(b); it reflects the overall predictive accuracy of the stress–strain curve. It is discovered that Crack-Net accurately predicts the specific work, achieving an R^2 value of 0.736. This result underscores Crack-Net's effectiveness in addressing non-convex energy evolution problems.

The reference and prediction fracture process from the PRC specimen (Fig. 5(c)) and IPCs (Fig. 5(d)) were compared, and good agreement was found. The results reveal that, despite the significant complexities arising from the presence of interfaces and diverse initial conditions, our approach demonstrates remarkable data efficiency.

3.4. Transfer learning in stiff and soft fillers

In real epoxy composite systems, inorganic fillers always present a much higher modulus compared with the matrix, while elastomer fillers are much softer (several to tens of megapascals). For this reason, cases of stiff fillers ($E_B = 50$ GPa, $S_B = 112$ MPa, $g_{CB} = 10$ J·m⁻²) and soft fillers ($E_B = 100$ MPa, $S_B = 4.8$ MPa, $g_{CB} = 10$ J·m⁻²) are examined in Fig. 6. It is important to clarify that these specific values are selected for illustrative purposes only; the method is applicable to fillers with any E_B value, regardless of their stiffness or softness. To reduce the demand for the training dataset, transfer learning was adopted here to leverage the knowledge learned from the last section and adapt it to the current scenarios, as shown in Fig. 6(a).

Fig. 6(b) demonstrates the transfer learning performance of Crack-Net on weak fillers with $S_B = 4.8$ MPa and $E_B = 100$ MPa. In the transfer learning, 120 cases with different composite morphologies were adopted as the dataset to fine-tune the model. Detailed settings for the training process are discussed in Section 2. Out-of-sample tests were conducted for both the transfer learning model (Model T) and the source model without transfer learning (Model N). It is worth noting that the two representative crack patterns were selected from the peak stress point and failure point, respectively; curve R denotes the curve from the reference, curve T denotes that from the transfer learning (Model T), and curve N denotes that from the no transfer learning (Model N), respectively. Similarly, transfer learning was applied to composites with strong fillers (Fig. 6(c), $S_B = 112$ MPa and $E_B = 50$ 000 MPa). The training

dataset also consisted of 120 cases, and the training setting remained the same. The experimental outcomes demonstrated the effectiveness of transfer learning in increasing the model's predictive generalization ability. In contrast, the source model's predictions were entirely incorrect, indicating a lack of predictive ability. The results also confirm that the model's predictive ability can be successfully transferred to diverse scenarios featuring different fillers, provided that the main model has been trained on the source domain.

3.5. Crack propagation in an elastoplastic matrix reinforced by stiff and strong fillers

The above investigations focused on the prediction of brittle crack growth in elastic materials. This deviates from a real-world situation, however, since plastic deformation is important to the fracture of epoxy composites. In the case of brittle fractures, the driving force for failure is tensile stress; accordingly, the typical crack pattern is a single crack propagating perpendicularly in the loading direction, which is easy to predict. However, in the presence of plasticity, the shear strain will extensively localize on narrow zones called shear yielding bands, where the materials are severely damaged, and failure can subsequently occur. In notched composite specimens with stiff particles, the stiff particles can induce a stress concentration at the interface, and the shear yielding bands can be highly branched (Fig. 7(a)), leading to an intricate crack evolution process. Considering that a shear yielding band is an important toughening mechanism in inorganic filler reinforced epoxy composites [63–65], being able to predict the shear yielding band, as well as the crack propagation path, is equally crucial.

In this section, an elastoplastic matrix with a yielding stress of 30 MPa was applied ($Y_A = 30$ MPa). The hardening modulus was assumed to be zero. The stress is expected to increase and then remain at 30 MPa until rupture, indicating that the tensile strength of the matrix is also 30 MPa ($S_A = 30$ MPa). The modulus and fracture parameter were kept the same as the values in the elastic cases ($E_A = 5$ GPa, $g_{CA} = 10$ J·m⁻²). Moreover, a stiff and strong filler was used ($E_B = 50$ GPa, $S_B = 110$ MPa, $g_{CB} = 10$ J·m⁻²), referring to the inorganic particles that are always used in high-modulus scenarios. Both a strong interface ($E_{IF} = 5000$ MPa, $g_{CIF} = 10$ J·m⁻², $S_{IF} = 35.0$ MPa) and a weak interface ($E_{IF} = 5000$ MPa, $g_{CIF} = 1$ J·m⁻², $S_{IF} = 10.8$ MPa) were examined. The filler and interface were considered to be elastic, and a new input layer Y_c was used to critically distinguish elastic behaviors (value = 0) and elastoplastic behaviors (value = 1) in materials

In the reference of the strong interface case (Fig. 7(a)), three representative points are extracted from the stress–strain curve, and the patterns of d_{k+1} and $\Delta d'_k$ are presented. At stress peak point R1, the maximum crack phase field value is less than 1, indicating that crack initiation has not yet occurred, and the subsequent stress decline is attributed to the overall shear deformation of the specimen. Accordingly, an intricate $\Delta d'_k$ pattern induced by highly branched shear yielding bands can be seen. By stretching the specimen to the R2 point, the crack starts to grow, and the stress declines. The pattern of $\Delta d'_k$ is no longer highly branched but bifurcated at the pre-crack tip, because the dominant shear yielding is induced by the pre-crack rather than the matrix-particle interface. At the final rupture point R3, the destructive crack is presented on one of the dominant shear yielding bands, and the specimen fails. The cosine similarity of the predicted crack under different strains and the predicted specific work are presented in Fig. 7(b). Although the fracture process is much more complicated, Crack-Net made impressive predictions—not only of the stress–strain curve but also regarding the crack evolution, even when shear yielding bands existed.

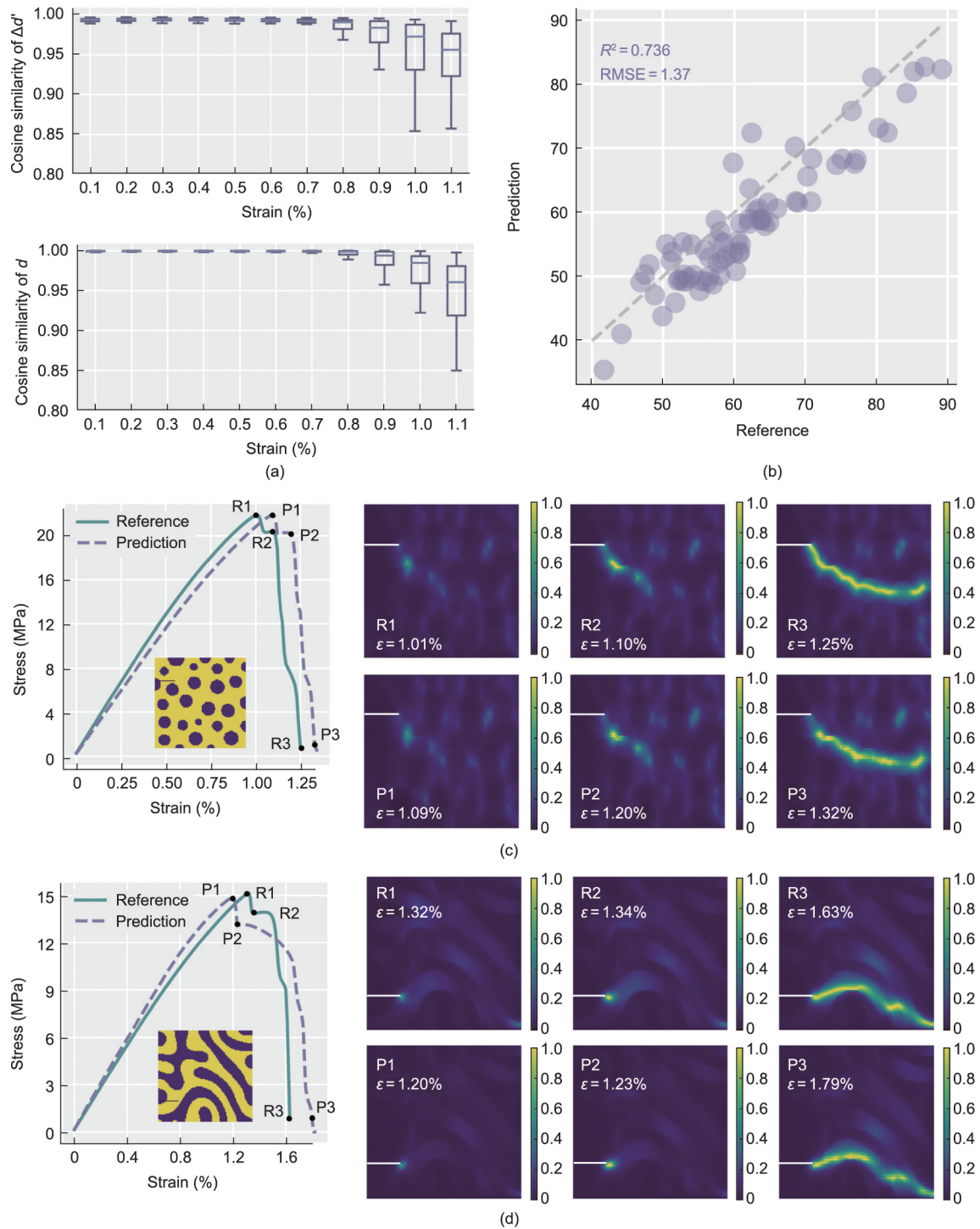


Fig. 5. The prediction by Crack-Net under poor interfacial adhesion and random initial cracks. (a) Cosine similarity of crack phase field d and transformed incremental value $\Delta d'$ under different strains. The purple line refers to the median. (b) Prediction and reference for the specific work of the stress–strain curve. (c, d) The composite morphology, the predicted and referred stress–strain curve (left), and the reference (R1–R3) and prediction (P1–P3) of the crack phase field at representative points for the (c) PRC specimen and (d) IPCs specimen with interface and varying initial conditions.

In Figs. 7(c) and (d), when the interface is weak, the crack still propagates on the shear yielding bands induced by the pre-cracking, but the bands induced by the interface are greatly weakened because of its poor strength. Alternatively, the weak interface acts as debonding points and accelerates the crack propagation (R2 point). This transition of the interface from shear yielding points to debonding points was successfully captured by the model by leveraging transfer learning.

4. Conclusion

This work proposed a deep-learning framework called Crack-Net to predict the fracture process in particulate epoxy composites. The hierarchical architecture of Crack-Net makes it able to learn the underlying relationship between crack evolution and stress response, which grants it enhanced predictive accuracy and physical consistency with less data requirement. Numerical experiments

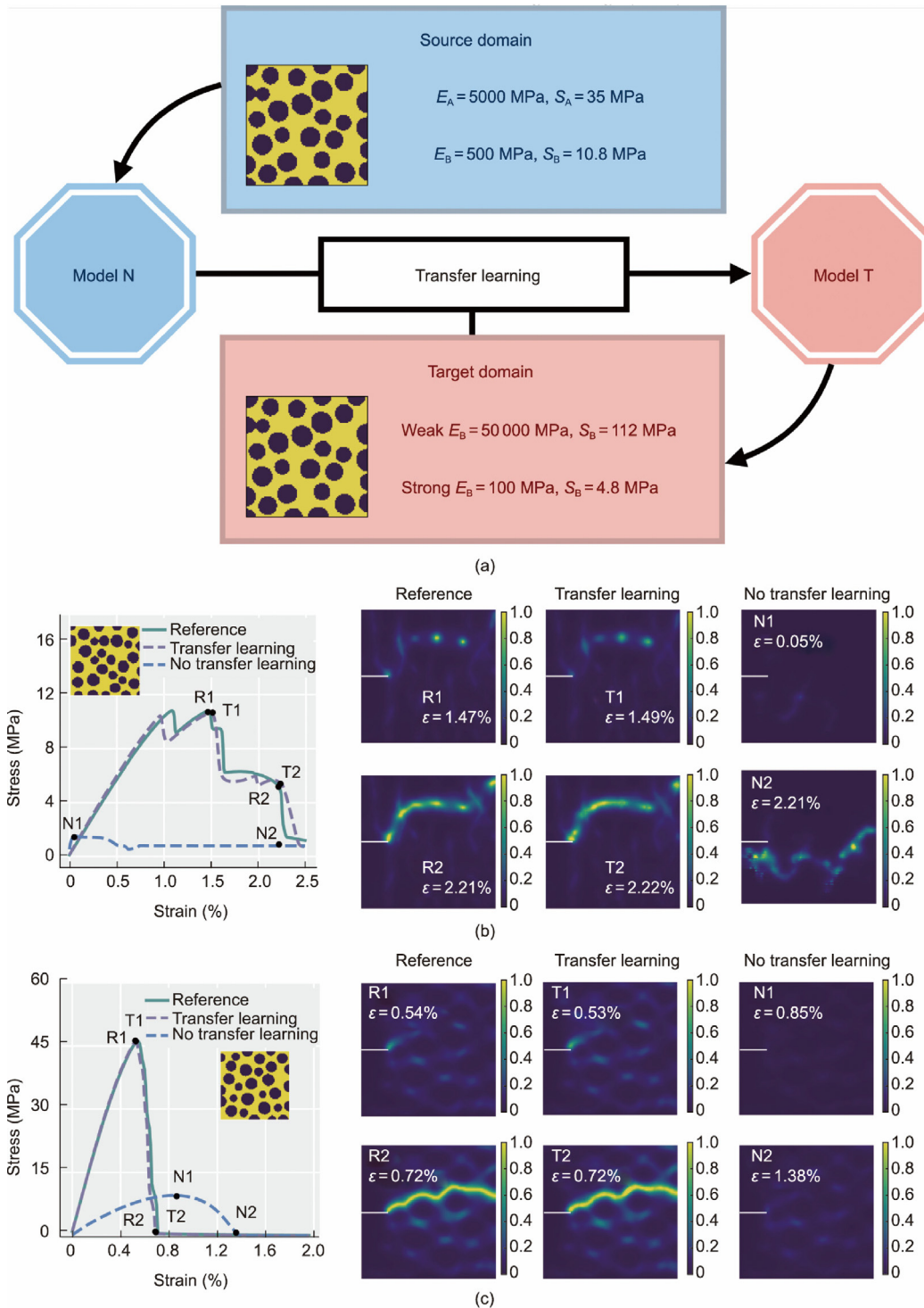


Fig. 6. Illustration and outcomes for Crack-Net’s transfer learning. (a) Schematic of transfer learning: Model T inherits knowledge from Model N and is then fine-tuned by the data from the target domain. (b, c) The outcomes of transfer learning for the composites with (b) weak fillers and (c) strong fillers. Unit: MPa.

demonstrated that Crack-Net can address intricate scenarios that encompass diverse interfaces, varying initial conditions, and the intricate elastoplastic fracture process. Under these conditions, Crack-Net accurately predicts the whole fracture evolution process, in addition to the stress–strain curve for a given microstructure.

Although Crack-Net does not achieve the precision of FEMs, which seamlessly incorporate complex boundary conditions and geometries, it demonstrates a certain degree of flexibility. For example, a case of mixed loading conditions is discussed in

Section S1.5 in Appendix A, highlighting Crack-Net’s capability to manage complex scenarios, although it is still in a nascent stage. It is important to clarify that the aim of this research is not to completely supplant traditional simulation methods but rather to find a balance between computationally intensive models (e.g., FEM) and data-heavy approaches (e.g., DNNs).

Although data-driven methods, such as DNNs, have made great progress in modeling fracture behaviors, a vast amount of data is required for training static prediction models, which usually

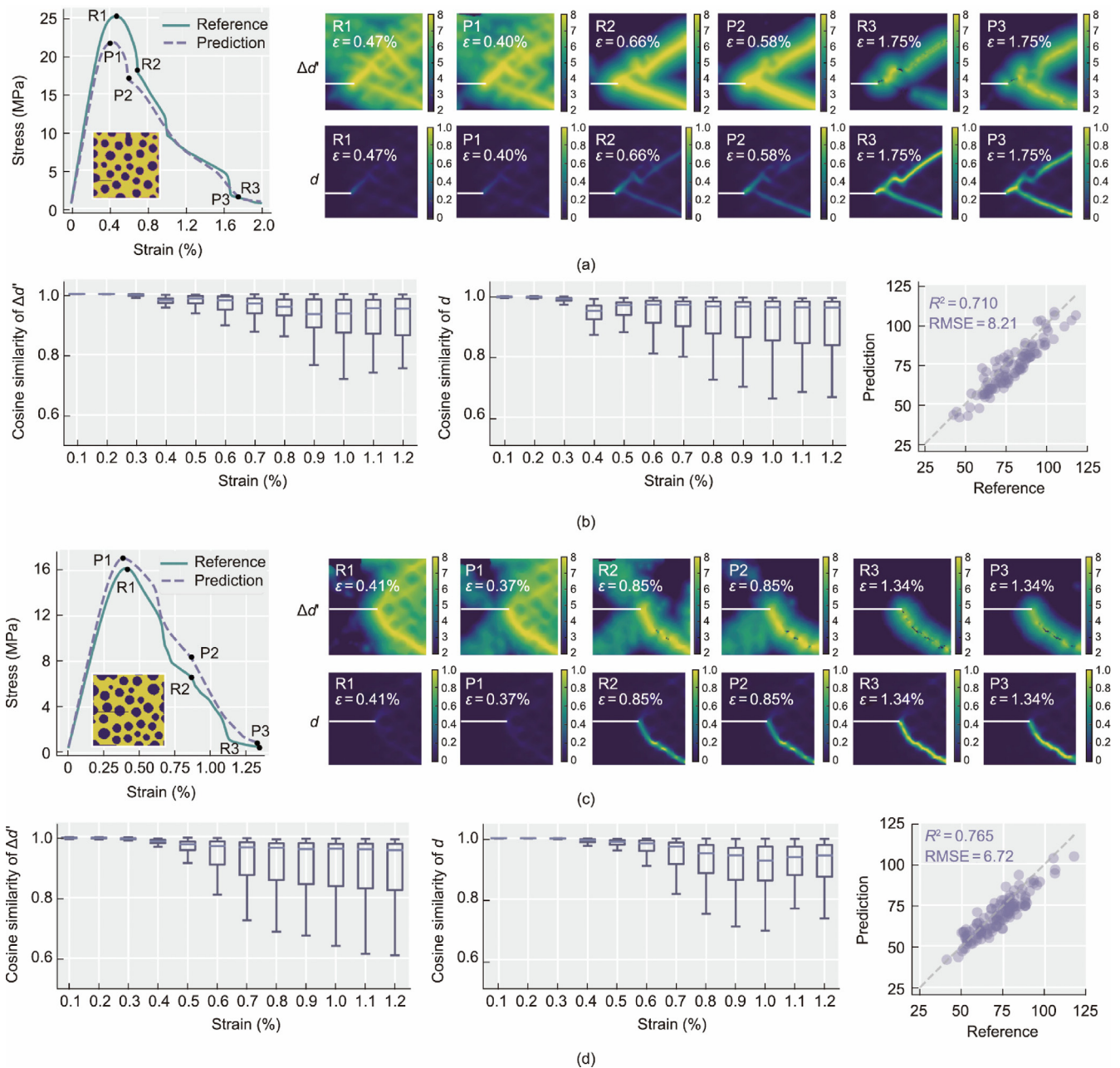


Fig. 7. Extension to the prediction of an elastoplastic matrix reinforced by stiff and strong fillers. (a) Predicted and referred stress–strain curve (left), and the reference (R1–R3) and prediction (P1–P3) of the transformed incremental value $\Delta d'$ (upper) and crack phase field d (lower) at representative points for an elastoplastic matrix with a strong interface. (b) Cosine similarity of transformed incremental value $\Delta d'$ and crack phase field d under different strains (left) and the prediction and reference for the specific work of the stress–strain curve (right). The purple line refers to the median. (c) Predictions of Crack-Net and references at representative points for the elastoplastic matrix with a weak interface. (d) Cosine similarity of transformed incremental value $\Delta d'$ and crack phase field d under different strains (left), and the prediction and reference for the specific work of the stress–strain curve (right).

predict the final state rather than the entire process. However, acquiring data from both numerical simulation and physical experiments is costly in terms of time and labor, rendering these data-driven models inefficient. PINNs manage to reduce the data requirements and improve prediction accuracy in homogeneous scenarios by incorporating explicit physical constraints. Their performance, however, is significantly constrained because of the non-convex feature and discontinuous solutions in composites, as discussed above. Moreover, incorporating the explicit physical constraints into the loss function of the network will complicate the optimization process, significantly increasing the computational costs. In contrast, Crack-Net achieves a balance between data-

driven and knowledge-driven techniques by incorporating the underlying relationship between crack propagation and stress response into the network architecture. This enables Crack-Net to inherently navigate the inner nonlinearities by combining a short-term data-driven solver with long-term physical insights. This approach not only facilitates accurate predictions of stress–strain relationships and crack evolution at the same time but also constitutes a promising method for balancing computational modeling.

Crack-Net’s applications extend beyond particulate epoxy composites to include particle-reinforced metallic and ceramic materials. Despite the distinct mechanical properties of these materials in

comparison with polymers, the underlying fracture principle and toughening mechanisms remain consistent. More importantly, Crack-Net represents a scalable approach to potentially predict the mechanics of heterogeneous structures including—but not limited to—bioinspired “brick-and-mortar” hierarchical materials, 3D-printed IPCs, and fiber-reinforced epoxies, as long as the simulation model is adjusted properly. Ongoing efforts are expanding Crack-Net’s utility in scenarios involving the crystal plasticity finite-element method (CPFE), with preliminary results affirming its broad applicability. Some limitations, however, remain in Crack-Net. For example, the interface between the matrix and fibers is treated and simulated on the basis of ideal assumptions, while practical situations may be more complex. In addition, the fracture processing zone plays a crucial role in fracture mechanics, yet capturing its characteristics necessitates an exceptionally refined element size. Given the considerable computational expense associated with generating the necessary data, it has not been incorporated into the current analysis. Future work may concentrate on combining the implicit and explicit constraints to further enhance the predictive capability of the proposed model.

CRedit authorship contribution statement

Hao Xu: Writing – review & editing, Writing – original draft, Visualization, Validation, Software, Methodology, Investigation, Formal analysis, Data curation, Conceptualization. **Wei Fan:** Writing – review & editing, Writing – original draft, Software, Investigation, Formal analysis, Conceptualization. **Lecheng Ruan:** Methodology, Investigation. **Rundong Shi:** Investigation, Formal analysis. **Ambrose C. Taylor:** Writing – review & editing, Supervision, Resources, Conceptualization. **Dongxiao Zhang:** Writing – review & editing, Writing – original draft, Supervision, Resources, Project administration, Investigation, Conceptualization.

Declaration of competing interest

The authors declare that they have no known competing financial interests or personal relationships that could have appeared to influence the work reported in this paper.

Acknowledgments

This work is supported and partially funded by the National Natural Science Foundation of China (52288101) and the China Postdoctoral Science Foundation (2024M761535). This work is also supported by the High Performance Computing Centers at Eastern Institute of Technology, Ningbo, and Ningbo Institute of Digital Twin.

Appendix A. Supplementary data

Supplementary data to this article can be found online at <https://doi.org/10.1016/j.eng.2025.02.022>.

References

- [1] Mi X, Liang N, Xu H, Wu J, Jiang Y, Nie B, et al. Toughness and its mechanisms in epoxy resins. *Prog Mater Sci* 2022;130:100977.
- [2] Fan W, Yang H, Taylor AC. Numerical analysis of fracture in interpenetrating phase composites based on crack phase field model. *Compos Sci Technol* 2023;232:109873.
- [3] Lin L, Wang Y, Lin Z, Luo W, Zhang H, Chen G, et al. A simplified reinforcement and fracture mechanism analysis model of epoxy nanocomposites based on finite element simulation. *Polymer* 2022;250:124879.
- [4] Andraju LB, Raju G. Continuum and cohesive zone damage models to study intra-laminar failure of curved composite laminates under four-point bending. *Compos Struct* 2020;253:112768.

- [5] Hu X, Chen W, Zhang P, Bui TQ, Yao W. A new crack-tip singular element for cracks in three-dimensional elastic bodies. *Eng Fract Mech* 2020;235:107148.
- [6] Dionísio JMM, Ramalho LDC, Sánchez-Arce IJ, Campilho RDSG, Belinha J. Fracture mechanics approach to stress singularities in composite adhesive joints. *Compos Struct* 2021;276:114507.
- [7] Wang X, Zhang J, Wang Z, Liang W, Zhou L. Finite element simulation of the failure process of single fiber composites considering interface properties. *Compos B Eng* 2013;45:573–80.
- [8] Ma S, Zhang X, Chen T, Wang X. Microstructure-based numerical simulation of the mechanical properties and fracture of a Ti-Al₃Ti core-shell structured particulate reinforced A356 composite. *Mater Des* 2020;191:108685.
- [9] Samaras G, Bikos D, Skamniotis C, Cann P, Masen M, Hardsalupas Y, et al. Experimental and computational models for simulating the oral breakdown of food due to the interaction with molar teeth during the first bite. *Extreme Mech Lett* 2023;62:102047.
- [10] Samaras G, Bikos D, Cann P, Masen M, Hardsalupas Y, Vieira J, et al. A multiscale finite element analysis model for predicting the effect of micro-aeration on the fragmentation of chocolate during the first bite. *Eur J Mech A-Solid* 2024;104:105221.
- [11] Dimitri R, Fantuzzi N, Li Y, Tornabene F. Numerical computation of the crack development and SIF in composite materials with XFEM and SFEM. *Compos Struct* 2017;160:468–90.
- [12] Zhao L, Zhi J, Zhang J, Liu Z, Hu N. XFEM simulation of delamination in composite laminates. *Compos Part A Appl Sci Manuf* 2016;80:61–71.
- [13] Swati RF, Wen LH, Elahi H, Khan AA, Shad S. Extended finite element method (XFEM) analysis of fiber reinforced composites for prediction of micro-crack propagation and delaminations in progressive damage: a review. *Microsystem Technologies* 2019;25:747–63.
- [14] Quinteros L, García-Macías E, Martínez-Pañeda E. Micromechanics-based phase field fracture modelling of CNT composites. *Compos B Eng* 2022;236:109788.
- [15] Tan W, Martínez-Pañeda E. Phase field predictions of microscopic fracture and R-curve behaviour of fibre-reinforced composites. *Compos Sci Technol* 2021;202:108539.
- [16] Bui TQ, Hu X. A review of phase-field models, fundamentals and their applications to composite laminates. *Eng Fract Mech* 2021;248:107705.
- [17] Fan W, Yang H, Mao S, Xin Z, Taylor AC. Numerical analysis of fracture in core-shell particle reinforced composites. *Compos Sci Technol* 2024;250:110536.
- [18] Greco F, Leonetti L, Luciano R, Nevone BP. Effects of microfracture and contact induced instabilities on the macroscopic response of finitely deformed elastic composites. *Compos B Eng* 2016;107:233–53.
- [19] Nguyen VP, Lloberas-Valls O, Stroeven M, Sluys LJ. Computational homogenization for multiscale crack modeling. Implementational and computational aspects. *Int J Numer Methods Eng* 2012;89:192–226.
- [20] Belytschko T, Song JH. Coarse-graining of multiscale crack propagation. *Int J Numer Methods Eng* 2010;81:537–63.
- [21] Toro S, Sánchez PJ, Blanco PJ, De Souza Neto EA, Huespe AE, Feijóo RA. Multiscale formulation for material failure accounting for cohesive cracks at the macro and micro scales. *Int J Plast* 2016;76:75–110.
- [22] Ghosh S, Lee K, Raghavan P. A multi-level computational model for multi-scale damage analysis in composite and porous materials. *Int J Solids Struct* 2001;38(14):2335–85.
- [23] Buryachenko VA. Peridynamic micromechanics of composites: a review. *J Peridyn Nonlocal Model* 2024;6:531–601.
- [24] Yang Z, Zheng S, Han F, Cui J. An efficient peridynamics-based statistical multiscale method for fracture in composite structures. *Int J Mech Sci* 2023;259:108611.
- [25] Mozaffar M, Bostanabad R, Chen W, Ehmann K, Cao J, Bessa MA. Deep learning predicts path-dependent plasticity. *Proc Natl Acad Sci USA* 2019;116:26414–20.
- [26] Liu B, Kovachki N, Li Z, Azizadenehsheli K, Anandkumar A, Stuart AM, et al. A learning-based multiscale method and its application to inelastic impact problems. *J Mech Phys Solids* 2022;158:104668.
- [27] Daghighi V, Lacy TE, Daghighi H, Gu G, Baghaei KT, Horstemeyer MF, et al. Machine learning predictions on fracture toughness of multiscale bio-nano-composites. *J Reinf Plast Compos* 2020;39:587–98.
- [28] Rahman A, Deshpande P, Radue MS, Odegard GM, Gowtham S, Ghosh S, et al. A machine learning framework for predicting the shear strength of carbon nanotube-polymer interfaces based on molecular dynamics simulation data. *Compos Sci Technol* 2021;207:114587.
- [29] Yamanaka A, Kamijyo R, Koenuma K, Watanabe I, Kuwabara T. Deep neural network approach to estimate biaxial stress-strain curves of sheet metals. *Mater Des* 2020;195:108970.
- [30] Yan S, Zou X, Ilkhani M, Jones A. An efficient multiscale surrogate modelling framework for composite materials considering progressive damage based on artificial neural networks. *Compos B Eng* 2020;194:108014.
- [31] Yang C, Kim Y, Ryu S, Gu GX. Prediction of composite microstructure stress-strain curves using convolutional neural networks. *Mater Des* 2020;189:1–9.
- [32] Kim DJ, Kim GW, Baek Jh, Nam B, Kim HS. Prediction of stress-strain behavior of carbon fabric woven composites by deep neural network. *Compos Struct* 2023;318:117073.
- [33] Ammasai SG. Prediction of two-phase composite microstructure properties through deep learning of reduced dimensional structure-response data. *Compos B Eng* 2021;225:109282.

- [34] Liu Z, Wu CT, Koishi M. A deep material network for multiscale topology learning and accelerated nonlinear modeling of heterogeneous materials. *Comput Methods Appl Mech Eng* 2019;345:1138–68.
- [35] Kim DW, Go MS, Lim JH, Lee S. Data-driven stress and strain curves of the unidirectional composites by deep neural networks with principal component analysis and selective-data augmentation. *Compos Struct* 2023;313:116902.
- [36] Zhang Z, Liu Q, Wu D. Predicting stress–strain curves using transfer learning: knowledge transfer across polymer composites. *Mater Des* 2022;218:110700.
- [37] Sepasdar R, Karpatne A, Shakiba M. A data-driven approach to full-field nonlinear stress distribution and failure pattern prediction in composites using deep learning. *Comput Methods Appl Mech Eng* 2022;397:115126.
- [38] Bhaduri A, Gupta A, Graham-Brady L. Stress field prediction in fiber-reinforced composite materials using a deep learning approach. *Compos B Eng* 2022;238:109879.
- [39] Yang Z, Yu CH, Buehler MJ. Deep learning model to predict complex stress and strain fields in hierarchical composites. *Sci Adv* 2021;7(15):eabd7416.
- [40] Khorrami MS, Mianroodi JR, Siboni NH, Goyal P, Svendsen B, Benner P, et al. An artificial neural network for surrogate modeling of stress fields in viscoplastic polycrystalline materials. *NPJ Comput Mater* 2023;9:37.
- [41] Chen Y, Dodwell T, Chuaqui T, Butler R. Full-field prediction of stress and fracture patterns in composites using deep learning and self-attention. *Eng Fract Mech* 2023;286:109314.
- [42] Ding X, Hou X, Xia M, Ismail Y, Ye J. Predictions of macroscopic mechanical properties and microscopic cracks of unidirectional fibre-reinforced polymer composites using deep neural network (DNN). *Compos Struct* 2022;302:116248.
- [43] Font-Clos F, Zanchi M, Hiemer S, Bonfanti S, Guerra R, Zaiser M, et al. Predicting the failure of two-dimensional silica glasses. *Nat Commun* 2022;13:1–11.
- [44] Rao C, Ren P, Wang Q, Buyukozturk O, Sun H, Liu Y. Encoding physics to learn reaction–diffusion processes. *Nat Mach Intell* 2023;5:765–79.
- [45] Kirchdoerfer T, Ortiz M. Data-driven computational mechanics. *Comput Methods Appl Mech Eng* 2016;304:81–101.
- [46] Carrara P, De Lorenzis L, Stainier L, Ortiz M. Data-driven fracture mechanics. *Comput Methods Appl Mech Eng* 2020;372:113390.
- [47] Wang J, Mo YL, Izzuddin B, Kim CW. Exact dirichlet boundary physics-informed neural network EPINN for solid mechanics. *Comput Methods Appl Mech Eng* 2023;414:116184.
- [48] Samaniego E, Anitescu C, Goswami S, Nguyen–Thanh VM, Guo H, Hamdia K, et al. An energy approach to the solution of partial differential equations in computational mechanics via machine learning: concepts, implementation and applications. *Comput Methods Appl Mech Eng* 2020;362:112790.
- [49] Zheng B, Li T, Qi H, Gao L, Liu X, Yuan L. Physics-informed machine learning model for computational fracture of quasi-brittle materials without labelled data. *Int J Mech Sci* 2022;223:107282.
- [50] Goswami S, Yin M, Yu Y, Karniadakis GE. A physics-informed variational DeepONet for predicting crack path in quasi-brittle materials. *Comput Methods Appl Mech Eng* 2022;391:114587.
- [51] Goswami S, Anitescu C, Chakraborty S, Rabczuk T. Transfer learning enhanced physics informed neural network for phase-field modeling of fracture. *Theor Appl Fract Mech* 2020;106:102447.
- [52] Haghghat E, Raissi M, Moure A, Gomez H, Juanes R. A physics-informed deep learning framework for inversion and surrogate modeling in solid mechanics. *Comput Methods Appl Mech Eng* 2021;379:113741.
- [53] Henkes A, Wessels H, Mahnken R. Physics informed neural networks for continuum micromechanics. *Comput Methods Appl Mech Eng* 2022;393:114790.
- [54] Cahn JW, Hilliard JE. Free energy of a nonuniform system II. Thermodynamic basis. *J Chem Phys* 1959;30:1121–4.
- [55] Logg A, Wells GN. DOLFIN: automated finite element computing. *ACM T Math Software* 2010;37(2):1–28.
- [56] Logg A, Mardal KA, Wells GN, editors. Automated solution of differential equations by the finite element method. Heidelberg: Springer Berlin; 2012.
- [57] Molnár G, Gravouil A, Seghir R, Réthoré J. An open-source Abaqus implementation of the phase-field method to study the effect of plasticity on the instantaneous fracture toughness in dynamic crack propagation. *Comput Methods Appl Mech Eng* 2020;365:113004.
- [58] Zhou Z, Rahman Siddiquee MM, Tajbakhsh N, Liang J. UNet++: a nested U-NET architecture for medical image segmentation. In: *Lecture notes in computer science*. Cham: Springer; 2018. p. 3–11.
- [59] Ronneberger O, Fischer P, Brox T. U-Net: convolutional networks for biomedical image segmentation. In: *Lecture notes in computer science*. Cham: Springer; 2015. p. 234–41.
- [60] Pan SJ, Yang Q. A survey on transfer learning. *IEEE Trans Knowl Data Eng* 2010;22(10):1345–59.
- [61] Feo L, Greco F, Leonetti L, Luciano R. Mixed-mode fracture in lightweight aggregate concrete by using a moving mesh approach within a multiscale framework. *Compos Struct* 2015;123:88–97.
- [62] Chen J, Taylor AC. Epoxy modified with triblock copolymers: morphology, mechanical properties and fracture mechanisms. *J Mater Sci* 2012;47:4546–60.
- [63] Lee J, Yee AF. Fracture of glass bead/epoxy composites: on micro-mechanical deformations. *Polymer* 2000;41:8363–73.
- [64] Akbari B, Bagheri R. Deformation mechanism of epoxy/clay nanocomposite. *Eur Polym J* 2007;43:782–8.
- [65] Canal LP, Segurado J, Llorca J. Failure surface of epoxy-modified fiber-reinforced composites under transverse tension and out-of-plane shear. *Int J Solids Struct* 2009;46:2265–74.